

Smooth Surface Reconstruction Using Tensor Fields as Structuring Elements

M. B. Vieira¹, P. P. Martins Jr.², A. A. Araújo³, M. Cord⁴ and S. Philipp-Foliguet⁴

¹ IMPA—Instituto de Matemática Pura e Aplicada, Est. Dona Castorina, 110, 22460-320, Rio de Janeiro, RJ, Brazil

² Centro Tecnológico de Minas Gerais, av. José Cândido da Silveira, 2000, 31170-000, Belo Horizonte, MG, Brazil

³ NPDI/DCC—Universidade Federal de Minas Gerais, Caixa Postal 702, 30161-970, Belo Horizonte, MG, Brazil

⁴ Ecole Nationale Supérieure d'Electronique et de ses Applications, 6 av. du Ponceau, 95014, Cergy Cedex, France

Abstract

We propose a new strategy to estimate surface normal information from highly noisy sparse data. Our approach is based on a tensor field morphologically adapted to infer normals. It acts as a three-dimensional structuring element of smooth surfaces. Robust orientation inference for all input elements is performed by morphological operations using the tensor field. A general normal estimator is defined by combining the inferred normals, their confidences and the tensor field. This estimator can be used to directly reconstruct the surface or give input normals to other reconstruction methods. We present qualitative and quantitative results to show the behavior of the original methods and ours. A comparative discussion of these results shows the efficiency of our propositions.

Keywords: normal estimation, surface reconstruction, organization inference, extremal surfaces, orientation tensor, morphological operators.

ACM CCS: I.3.5 [Computer Graphics]: Geometric algorithms, languages and systems.

1. Introduction

Surface reconstruction concerns the problem of retrieving three-dimensional shapes which, in general, represent a physical object. In most cases, only points distributed over the object are known. Obtaining precise three-dimensional (3D) models of real objects has applications in reverse engineering, shape analysis, computer graphics and computer vision, among others.

The most important works on surface reconstruction classify a sparse cloud of points as an *unorganized point set* [1,2]. In Gopi and Krishnan [3], a set of points is classified *organized* if it has additional information about the original surface.

In the context of surface reconstruction, any sparse set of points is at least assumed to be *implicitly organized* since the points, or subsets of them, are structured by an arbitrary object. Outliers and additive noise can be present in real applications. In our work, organized points are

those that, within their neighborhood, are *structured over a surface*.

This notion of spatial organization may be seen as the lowest level in an organization scale that increases as the information about the underlying object becomes available. Geometric and topological information, for example, increase the organization level of independent point subsets.

From this point of view, *reconstruction* is the process of inferring more information about the underlying object. This is equivalent to reach higher levels in the organization scale for point sets. Performing high-level reconstruction is harder when information about the points organization is limited or missing. Precise normals associated to points, for example, make the surface reconstruction task easier.

Thus, estimating the surface's normal on input points is itself a reconstruction process that gives a higher level of organization to the data set. Resulting normals can further be used to reconstruct other types of information such as piecewise

surface approximation (an even higher organization level). Normal inference is the first surface reconstruction level.

This work focuses on the problem of robust normal estimation from a sparse and noisy set of points. Given a sparse data set, the first question is ‘what is the normal of the underlying surface in an arbitrary point P ?’, where P is not restricted to the input points. The second question is ‘how good is this normal estimation?’ Points that do not belong to a surface are supposed to have poor estimation rates. The paper is organized as follows:

- Section 2 gives the introduction of related work and our contributions;
- Section 3 gives the description of the morphological operations for robust normal filtering and estimation;
- Section 4 gives the definition of a general normal estimator and surface reconstruction;
- Section 5 gives the comparative discussion based on qualitative and quantitative results.

This work is based on ‘Reconstruction Using Surface Dedicated Fensorial Fields’ which appeared in XVI Brazilian Symposium on Computer Graphics and Image Processing, © IEEE 2003.

2. Related Works

In Gideon Guy’s paradigm [4,5], surface reconstruction is performed by accumulating the orientation contributions of input elements using tensor fields. Guy essentially provides two functions $\mathbf{n}(D, Q) \rightarrow \mathbb{P}^2$ and $s(D, Q) \rightarrow \mathbb{R}^+$, where D is a sparse data set, $Q \in \mathbb{R}^3$ is an arbitrary point and \mathbb{P}^2 is the space of unoriented directions (projective two-sphere), in such a way that

- $\mathbf{n}(D, Q)$ is the estimation of a normal in Q representing a surface that presumably structures Q in conjunction with its neighborhood in D ;
- $s(D, Q)$ is the pertinence, or relevance degree of the normal estimate in comparison with the original object represented by D .

Set D may have points, with associated normal (surfels) and with associated tangent (curvels). Based on continuity constraints, Guy defined a 3D tensor field for each input class.

Using these fields, the structural contributions of each element are accumulated to infer normals $\mathbf{n}(D, P)$ and pertinences $s(D, P)$ for every $P \in D$. Next, the field for surfels is aligned with the inferred normal in every input point and the contributions are accumulated in the subspace containing D . Resulting tensors representing the subspace are decomposed and the surface and curves formed by the input points are retrieved by a local maxima extraction algorithm.

Lee and Medioni [6] extended Guy’s method using orientation tensors [7]. The main difference is that fields and

accumulation processes are based on tensor spectral decomposition rather than input classes. Curves formed by input points are retrieved using surface uncertainty obtained in tensors. This new approach gives better results than the original method but uncertainty propagation interferes negatively with surface reconstruction.

Note that the pertinence function does not provide any distance from the surface. Actually, it represents the likelihood of the inferred normal to be in fact over the surface. Extending or adapting the normal inference functions to use with state-of-art reconstruction algorithms is not only possible but promising.

For methods using radial basis functions, for example, our normal inference functions can, filter initial data and seed the algorithm with highly structured surfels, be part of the signed distance function and be used as simplification criteria for fast convergence [8,9].

2.1. Motivation

Guy’s method and its extensions are defined from a *perceptual point of view*. All propositions are based on the principles of computer vision. For example, they use circular connections to build their fields. The goal is to minimize the total curvature of the reconstructed surface, or curve, just like human’s perceptual system does.

Another important feature of previous works is that they explore the maximum of information that a tensor can represent. The methods are constructed in such a way that surfaces, curves and surface intersections can be extracted in a single- or a two-step accumulation process. However, the secondary information coded or resulted from tensor additions is better interpreted as uncertainty [7]. The interested reader will find valuable details in [5].

In our work, this reconstruction paradigm is perceived from a *morphological point of view*. We observed that the mathematical notions (fields and tensors) are explicitly combined to infer structural shapes. Thus, the tensor fields act as structuring elements in a morphological accumulation process. We propose general guidelines to reconstruct a specific structure considering this new perspective:

- tensor information should be coded and interpreted for the expected structure: sums of tensors have a limited but well-known behavior. A single tensor is an isolated structuring element and should code only the main structure’s information. Uncertainties of resulting tensors can be directly related to uncertainties about the structure’s localization;
- the tensor fields should be designed to be structuring elements of the expected structure: a tensor field can be defined from a vectorial field and a scalar field. The vectors define trajectories and the scalars define the confidence of the vector element. We emphasize that the trajectory of the scalar field gradient is very relevant;

- the morphological features of tensor fields should be exploited in the reconstruction process: different operators can be designed to obtain reliable information of a specific structure.

2.2. Contributions

Aiming the problem of normal estimation and its confidence from a sparse set of points, which is the essence of this reconstruction paradigm, our main contributions are:

- a tensor field morphologically adapted to infer normals: we combine a vectorial and a scalar field to form tensors that code only normal information. Both fields have elliptical trajectories (gradient of the scalar field) that can be adjusted to infer surface patches with varying curvatures;
- a morphological process that uses our tensor field to infer and enhance normal estimations: the tensor field is a structuring element of elliptical surfaces. Precise normals can be estimated when this field is properly aligned with input elements and then integrated in space.

The normal vectors and pertinences inferred by our method in conjunction with the normal tensor field form new functions $n(D, Q)$ and $s(D, Q)$ that give better first level organization estimations from highly noisy set D .

3. Robust Normal Estimation

We assume that an input set can have points and surfels. An isotropic tensor field to infer primary normals from points is needed. This initial inference can be then enhanced by our morphological method using the normal tensor field. Points with tangents can be treated as well [10]. The topics of this section are:

- orientation tensor codification and analysis;
- normal tensor field construction from elliptic vector and scalar fields;
- isotropic tensor field for primary inference;
- morphological normal estimation.

3.1. Orientation tensor

A symmetric second-order *orientation tensor* [7] is defined as

$$\mathbf{T} = \lambda_1 \mathbf{e}_1 \mathbf{e}_1^T + \lambda_2 \mathbf{e}_2 \mathbf{e}_2^T + \lambda_3 \mathbf{e}_3 \mathbf{e}_3^T, \quad (1)$$

where orientations are coded in the eigenvectors $\mathbf{e}_1 \perp \mathbf{e}_2 \perp \mathbf{e}_3$ with their respective eigenvalues $\lambda_1 \geq \lambda_2 \geq \lambda_3 \geq 0$ representing pertinences. It is used in three different ways in our method: coding, addition and interpretation.

All tensors in normal field have the desired normal coded in the eigenvector \mathbf{e}_1 , pertinence coded in λ_1 and $\lambda_2 = \lambda_3 = 0$. It means that no uncertainty is coded. The tensors of the isotropic field have planar uncertainty;

Normal inference is achieved by simply adding tensors. After aligning tensor fields with input points, the contribution of all elements are summed. Given two tensors \mathbf{A} and \mathbf{B} coding normal information, the addition $\mathbf{T} = \mathbf{A} + \mathbf{B}$ can be decomposed in three tensors [11]:

- normal information $(\lambda_1 - \lambda_2) \mathbf{e}_1 \mathbf{e}_1^T$ represents the collinearity of normals coded in \mathbf{A} and \mathbf{B} ;
- planar uncertainty $(\lambda_2 - \lambda_3)(\mathbf{e}_1 \mathbf{e}_1^T + \mathbf{e}_2 \mathbf{e}_2^T)$ gives the plane where the resulting normal is likely to be in;
- isotropic uncertainty $\lambda_3(\mathbf{e}_1 \mathbf{e}_1^T + \mathbf{e}_2 \mathbf{e}_2^T + \mathbf{e}_3 \mathbf{e}_3^T)$ represents the inability of finding a preferred normal direction, i.e. maximum uncertainty.

3.2. Normal tensor field

Aligned with an input element, a tensor field defines contributions in space. To derive a field that is morphologically adapted to infer normals forming smooth surfaces and balanced pertinences, we argue that:

- curvature adjustment augments the flexibility for general surface reconstruction: we use half ellipsoids but other structuring surfaces can be used as well;
- the orthogonal trajectory of the scalar field gradient should match the trajectory defined by the vector field: in our case, elliptic surfaces are imposed by both fields resulting in smoother normals.

The surface curvature may be controlled by using ellipses centered in the y -axis and tangent to the x -axis:

$$\frac{x^2}{t_x^2 k^2} + \frac{\left(-t_y + \frac{y}{k}\right)^2}{t_y^2} = 1, \quad (2)$$

where t_x and t_y are constants and k defines the ellipse having axis parallel to x and y with sizes $2kt_x$ and $2kt_y$, respectively. The ellipse shape defines the desired connections and can be easily controlled by the ratio of the axis sizes:

$$d = \frac{2kt_y}{2kt_x} = \frac{t_y}{t_x}, \quad (3)$$

which is constant for all ellipses of a family. Figure 1 shows some ellipse families with different values of d . The circular trajectory is obtained with $d = 1$.

Given a point $P \in \mathbb{R}^2$ with polar coordinates (ρ, θ) , the inclination of the line tangent to the ellipse passing by P is

$$\tan \beta = \frac{2d^2 \tan \theta}{d^2 - \tan^2 \theta}, \quad \cos \theta \neq 0, \quad d \neq |\tan \theta| \quad (4)$$

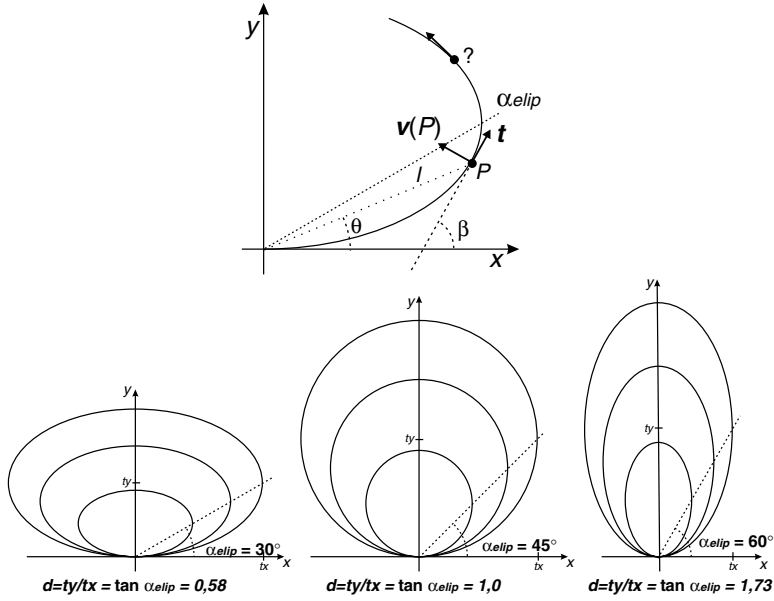


Figure 1: Ellipses with different shapes.

with β being the angle between this line and x -axis (Figure 1). When $|\tan \theta| = d$, the tangent line is perpendicular to the x -axis ($\beta = 90^\circ$), invalidating equation (4). No point can be connected to the origin beyond these ellipse extremities. They form the maximal connection angle α_{elip} (Figure 1) that defines the ellipse family by assigning

$$d = \tan \alpha_{\text{elip}}. \quad (5)$$

Consider a surfel $(P, \mathbf{k}) \in \mathbb{R}^3 \times \mathbb{S}^2$ and the unit vectors $\mathbf{i} \perp \mathbf{j}$, all arbitrary but perpendicular to \mathbf{k} . The point P and the orthonormal base $\{\mathbf{i}, \mathbf{j}, \mathbf{k}\}$ form a coordinate system in \mathbb{R}^3 (Figure 2). The spherical coordinates (ρ, ϕ, θ) of a point $Q \in \mathbb{R}^3$ are:

$$\rho = |PQ|, \quad \tan \phi = \frac{k}{\sqrt{i^2 + j^2}}, \quad \tan \theta = \frac{j}{i},$$

where $i = \mathbf{i} \cdot P\mathbf{Q}$, $j = \mathbf{j} \cdot P\mathbf{Q}$ and $k = \mathbf{k} \cdot P\mathbf{Q}$ are the cartesian coordinates of Q in the system (Figure 2). Equation (4) can be used to compute the angle β between the plane \mathbf{ij} and the tangent plane to the ellipsoid passing by Q :

$$\tan \beta = \frac{2d^2 \tan \phi}{d^2 - \tan^2 \phi},$$

$$\cos \phi \neq 0, \quad d = \tan \alpha_{\text{elip}}, \quad d \neq |\tan \phi|$$

where α_{elip} is the maximal connection angle. The 3D vectorial field for normals is defined by

$$\mathbf{v}_N((P, \mathbf{k}), Q) = (\mathbf{i} \cos \theta + \mathbf{j} \sin \theta) \cos \left(\beta + \frac{\pi}{2} \right) + \mathbf{k} \sin \left(\beta + \frac{\pi}{2} \right), \quad (6)$$

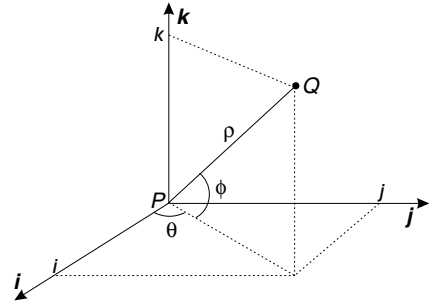


Figure 2: Spherical coordinates of a point Q in the coordinate system of a surfel (P, \mathbf{k}) .

where the addition of $\pi/2$ to β defines vectors normal to the ellipsoids.

The scalar gradient field representing the force, or induction capacity, of the tensors should define the same trajectory of the vectorial field. Thus, the equipotential surfaces of force must be orthogonal trajectories to the ellipsoids. We use the farthest distance from the origin of the orthogonal trajectory passing by Q :

$$f((P, \mathbf{k}), Q) = \rho \cos \phi \left(1 + \left(2 - \frac{1}{d^2} \right) \tan^2 \phi \right)^{\frac{d^2}{2d^2-1}}$$

as a norm for the ellipsoid passing by Q . Combined with a Gaussian, it forms the attenuated scalar field:

$$f_N((P, \mathbf{k}), Q) = e^{-\frac{f((P, \mathbf{k}), Q)^2}{\sigma^2}}$$

whose gradient vectors define the same trajectories of the vectorial field (equation (6)). The normal tensor field defining elliptical connections for a surfel (P, \mathbf{k}) in 3D is

$$\mathbf{C}_N((P, \mathbf{k}), Q) = \begin{cases} r\mathbf{v}\mathbf{v}^T, & \text{if } \phi \leq \alpha_{\max}, \\ \mathbf{0}, & \text{if } \phi > \alpha_{\max}, \end{cases}$$

$$\alpha_{\max} \leq \alpha_{\text{elip}}, \quad r = f_N((P, \mathbf{k}), Q), \quad \mathbf{v} = \mathbf{v}_N((P, \mathbf{k}), Q),$$

where α_{elip} defines the maximal angle and the curvature. The α_{\max} parameter can be used to define fields with smaller influence than α_{elip} .

If $\alpha_{\text{elip}} > 45^\circ$, more direct connections are allowed resulting in smoother surfaces. Reconstructions with $\alpha_{\text{elip}} < 45^\circ$ tend to preserve details but are more subject to noise. The best compromise between smoothness and detail preservation is obtained with spherical connections $\alpha_{\text{elip}} = 45^\circ$.

3.3. Isotropic Tensor Field

A point with no associated orientation $P \in \mathbb{R}^3$ has insufficient information to induce normals directly on another point Q . Guy showed that any plane passing by the straight line PQ is valid. The vectorial field defining this line

$$\mathbf{v}_I(P, Q) = \frac{PQ}{|PQ|}$$

is then used to code this planar uncertainty for normals. The force field should be radial and stronger for points near P :

$$f_I(P, Q) = e^{-\frac{|PQ|^2}{\sigma^2}}, \quad (7)$$

with attenuation factor σ . The isotropic tensor field in 3D is

$$\mathbf{C}_I(P, Q) = r(\mathbf{I} - \mathbf{v}\mathbf{v}^T), \quad r = f_I(P, Q), \quad \mathbf{v} = \mathbf{v}_I(P, Q),$$

where \mathbf{I} is the identity matrix. The plane containing the normal is defined by $\mathbf{e}_1\mathbf{e}_2$ with $\mathbf{e}_3 = \mathbf{v}_I(P, Q)$ (equation (1)). The force is coded in $\lambda_1 = \lambda_2 = f_I(P, Q)$ with $\lambda_3 = 0$.

3.4. Primary orientation inference

The primary inference is performed by the accumulation of the influence of all input points. Consider an input set D composed of i points and j surfels. To infer their orientations, every input point

$$\mathbf{Q}_m \in \{P_1, \dots, P_i\} \cup \{N_1, \dots, N_j\}, \quad 0 < m \leq i + j, \quad (8)$$

is associated to an orientation tensor $\mathbf{T}_m \in \{\mathbf{T}_1, \dots, \mathbf{T}_n\}$, $n = i + j$, representing the total influence of the sparse data D

$$\mathbf{T}_m = \sum_i \mathbf{C}_I(P_i, \mathbf{Q}_m) + \sum_j \mathbf{C}_N((N_j, \mathbf{n}_j), \mathbf{Q}_m).$$

Every tensor \mathbf{T}_m contains the inferred orientation for its corresponding point \mathbf{Q}_m from every input element of D .

The resulting vectors and pertinences coded in \mathbf{T}_m do not necessarily define smooth surfaces. Besides, noisy elements have the same weight of more precise elements.

3.5. Morphological normal estimation

The primary normal information contained in \mathbf{T}_m is highly subject to noise. As a result, these tensors are not suitable for surface reconstruction. This observation is a key difference between previous works and ours.

Considering that the normal tensor field is a *surface structuring element*, one may use it to improve normals at input elements. The normal information of an orientation tensor $\mathbf{A} = \lambda_1\mathbf{e}_1\mathbf{e}_1^T + \lambda_2\mathbf{e}_2\mathbf{e}_2^T + \lambda_3\mathbf{e}_3\mathbf{e}_3^T$ is given by functions

$$\mathbf{v}\mathbf{n}(\mathbf{A}) = \mathbf{e}_1, \quad s(\mathbf{A}) = \lambda_1 - \lambda_2,$$

where $\mathbf{v}\mathbf{n}$ is the normal vector and s is its pertinence.

A new tensor set $\mathbf{U}_m \in \{\mathbf{U}_1, \dots, \mathbf{U}_n\}$ is associated to the set of input points \mathbf{Q} and defined by the propagation of the normal information contained in \mathbf{T}_m :

$$\mathbf{U}_m = \sum_{l=1}^n s(\mathbf{T}_l)^\gamma \mathbf{C}_N((\mathbf{Q}_l, \mathbf{v}\mathbf{n}(\mathbf{T}_l)), \mathbf{Q}_m), \quad (9)$$

where $(\mathbf{Q}_l, \mathbf{v}\mathbf{n}(\mathbf{T}_l))$ is the tuple composed by n input points and their estimated normals.

The factor γ is used for pertinence regularization. If $\gamma \geq 1$, the difference among them is amplified. Elements with low pertinence tends to have lower influence, favoring noise filtering. This may generate holes in regions with low point density. If $\gamma < 1$, the difference between highest and lowest pertinences is reduced at exponential rate. In presence of noise, this may disturb reconstruction processes.

For general applications, we suggest to propagate the normal information twice (Figure 3). At first time, we estimate \mathbf{U}_m with $\gamma \geq 1$ to filter the primary orientations (equation (9)). Associating the tensor set $\mathbf{V}_m \in \{\mathbf{V}_1, \dots, \mathbf{V}_n\}$ to the set of input points \mathbf{Q} , the second normal propagation is given by

$$\mathbf{V}_m = \sum_{l=1}^n s(\mathbf{U}_l)^\omega \mathbf{C}_N((\mathbf{Q}_l, \mathbf{v}\mathbf{n}(\mathbf{U}_l)), \mathbf{Q}_m), \quad (10)$$

where $\omega < 1$ is the regularization factor. This second accumulation reduces the difference among the pertinences obtained in \mathbf{U}_m , also reducing the filtering effect in regions with low point density.

Two accumulations were effective to enhance the normal estimation but the process may be extended. Experiments show that $\gamma = 1$ and $\omega = 1/2$ provide good results in general applications.

High responses of normal estimation uncertainty may indicate noise presence. Thus, this information is discarded

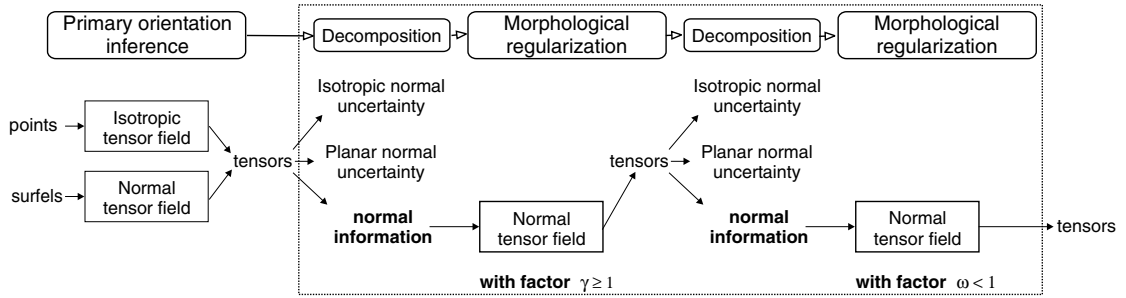


Figure 3: Morphological operator for robust normal estimation: normal tensor field as a surface structuring element.

within the morphological operator. We argue that uncertainties can be better analyzed from final tensors V_m .

Ideally, the sparse accumulation should assign maximal pertinence to the structured points and minimal to the unorganized ones. The more precise pertinence values provided by our functions tend to give greater pertinences to the organized points. This bimodal aspect of pertinence distribution enables the use of a threshold for segmenting both sets. In [2], we propose a method for sparse data filtering suitable for preprocessing purposes. In [3], we show the use of this filtering method in altimetry data to find vegetation regions.

4. Normal Inference Functions and Reconstruction

Using the normal tensor field and the orientation information obtained for all input elements, we define the general normal estimator for any point $P \in \mathbb{R}^3$

$$I(D, P) = \sum_{l=1}^n s(V_l) C_N((Q_l, \mathbf{v}n(V_l)), P), \quad (11)$$

where Q_l is the l th input point (equation (8)) and V_l is its orientation tensor obtained by morphological inference (equation (10)).

The decomposition of $I(D, P)$ provides the general normal inference functions $\mathbf{n} : D \times \mathbb{R}^3 \rightarrow \mathbb{P}^2$ and $s : D \times \mathbb{R}^3 \rightarrow \mathbb{R}^+$

$$\mathbf{n}(D, P) = \mathbf{e}_1 \quad \text{and} \quad s(D, P) = \lambda_1 - \lambda_2.$$

Function $I(D, P)$ defines a *continuum* of tensors in \mathbb{R}^3 . It can be used in several ways. For example, it could be attached to other types of reconstruction methods. Direct reconstruction can be performed by finding the *extremal surface* defined by

$$\mathbf{n}(D, P) \cdot \nabla s(D, P) = 0, \quad (12)$$

which is formed by the sites where the pertinence s is a local maxima in direction of the estimated normal vector \mathbf{n} .

The extremal surface notion has been revisited in [14] for reconstruction: they define the moving least square surface as an extremal surface.

4.1. Discrete case

Guy defined a variation of the marching cubes algorithm to extract extremal surfaces in a discrete grid. In this case, normals are inferred for every point $P \in S$ of a subspace $S \subset \mathbb{R}^3$ containing the input set D .

Subspace S is represented by a discrete grid of tensors $G_{i,j,k}$ with dimensions $r \times t \times u$ with $i, j, k, r, t, u \in \mathbb{Z}^+$. The evaluation of normals from subset D can be defined by applying $I(D, P)$ directly (equation 11)

$$G_{i,j,k} = I(D, H(i, j, k)), \quad i \leq r, \quad j \leq t, \quad k \leq u, \quad (13)$$

where function $H : \mathbb{Z}^{+3} \rightarrow \mathbb{R}^3$ is the transformation of discrete coordinates (i, j, k) , representing the center of the grid cell, into real coordinates corresponding to subspace S . A point $H(i, j, k)$ is over a surface if its pertinence s is a local maxima in direction of estimated normal vector \mathbf{n} (equation [12]).

In this work, the tensor grid $G_{i,j,k}$ is computed as defined above. However, this definition assumes that the grid has sufficient resolution to avoid or minimize *structural aliasing*.

In fact, our normal tensor field was designed for continuous normal reconstruction. It does not provide good results in the discrete pipeline of previous works. Thus, a discrete version taking into account the aliasing problem is needed. Discrete versions of normal inference functions must be defined carefully and is a subject for future works.

A probabilistic approach is to define a discrete normal tensor field where each element is the average of a random tensors inside its cell support. As a result, sites where normals are more aligned (plane \mathbf{ij} in Figure 2) would have higher final pertinence than those with varying curvature. This situation is empirically approximated by the force field defined by Lee and Medioni.

Note that applying the discrete field above is equivalent to take the average contribution of a points randomly chosen inside the grid cell with center (i, j, k) .

5. Experimental Results

We present qualitative and quantitative experiments to show the differences between the original methods and ours. Qualitative results allow the evaluation of reconstruction quality in challenging situations: insufficient grid resolution, high presence of outliers and complex surface intersections.

Obviously, the input data sets used for qualitative evaluation are single instances in an infinity of possible point distributions, each conducting to different results. The analysis of several reconstructions are needed to show the average behavior of the methods. In this way, a quantitative experiment comparatively shows the error evolution of all methods reconstructing ellipsoids.

The fixed parameters of each method were adjusted by comparison of several results in terms of reconstruction quality. We chose values that give best results for each one.

5.1. Qualitative results

For our method, we used $\gamma = 1$ (equation (9)) and $\omega = 1/2$ (equation (10)). Reconstructions with circular ($\alpha_{\text{elip}} = 45^\circ$) and elliptic ($\alpha_{\text{elip}} = 60^\circ$) continuities are given. Both with maximal angle $\alpha_{\text{max}} = 45^\circ$ (equation (7)) to reduce cross-talking between misaligned points.

For Guy's method, we set $a = 3$ and $b = 1$ to define a normalized force field between $-1 \leq x \leq 1$. Lee and Medioni method is applied with $c = 0.02$. See [5] for a complete description of these methods.

Fields should have finite support for performance purposes. The force may be considered null beyond a distance d_{max} from field's central point. To have coherent results, the force field parameters of all methods are adjusted in such a way that

$$f(P, Q) \leq k \forall Q \in \mathbb{R}^3 \mid |PQ| \geq d_{\text{max}}, \quad (14)$$

where P is the field's central point. Every point at distance d_{max} can have k as maximum force. The most aligned points have force k in anisotropic fields (like normal tensor field). We set $k = 0.001$ in this work.

A highly dense set of 10 000 points forming a knot model is given in Figure 4. The grid used for reconstruction is too restrictive due to the point's density and the object's complex topology. Several approaches would fail in reconstructing it.

The knot was reconstructed with $d_{\text{max}} = 0.06$ for our method and $d_{\text{max}} = 0.07$ for Lee and Guy methods. Our method with $\alpha_{\text{elip}} = 45^\circ$ and Lee and Guy methods were not able to extract the knot model correctly, resulting in several artifacts (Figure 4). However, almost all surface was correctly reconstructed with $\alpha_{\text{elip}} = 60^\circ$.

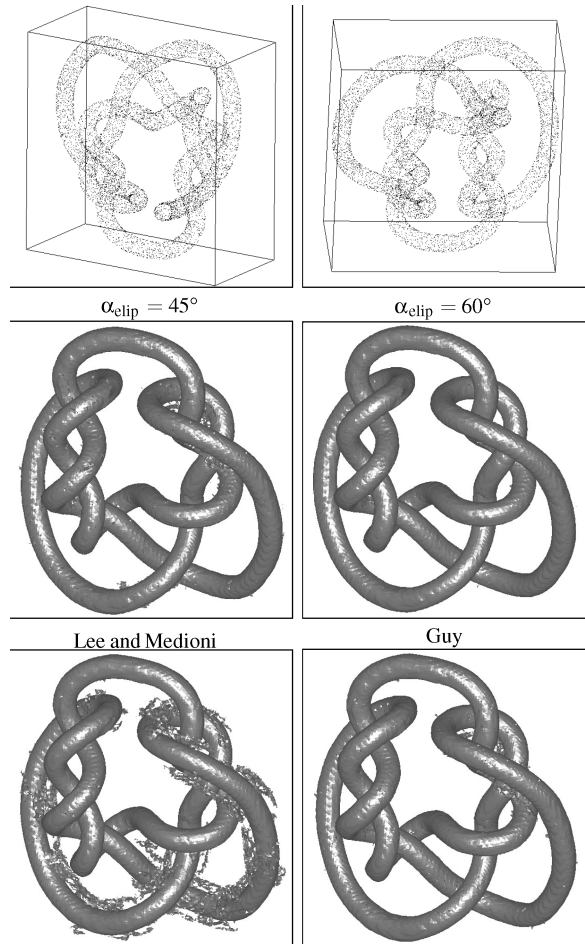


Figure 4: Complex data example: reconstruction of a knot's model in a restrictive grid of dimensions $130 \times 130 \times 65$.

Figure 5 shows 250 points forming a Cassini's oval with 1500 outliers uniformly distributed in the cube of side 15% greater than the cube containing the oval. This is an extremal case of outlier presence.

We used $d_{\text{max}} = 0.22$ for ours and Guy methods and $d_{\text{max}} = 0.21$ for Lee's. All methods extracted the object but only our method was able to reconstruct it entirely as a smooth surface (Figure 5). Similarly to the knot reconstruction, a smoother surface was obtained with $\alpha_{\text{elip}} = 60^\circ$ due to the elliptic curvature.

The cut views of Cassini's oval grid show that our method provides better results with noisy data (Figure 6). It reduces considerably the pertinences of unstructured points. This is due to our normal tensor field and the enhancement of the primary normal inference. Note that Lee and Medioni method is the most sensible to noise. Our method also gives more

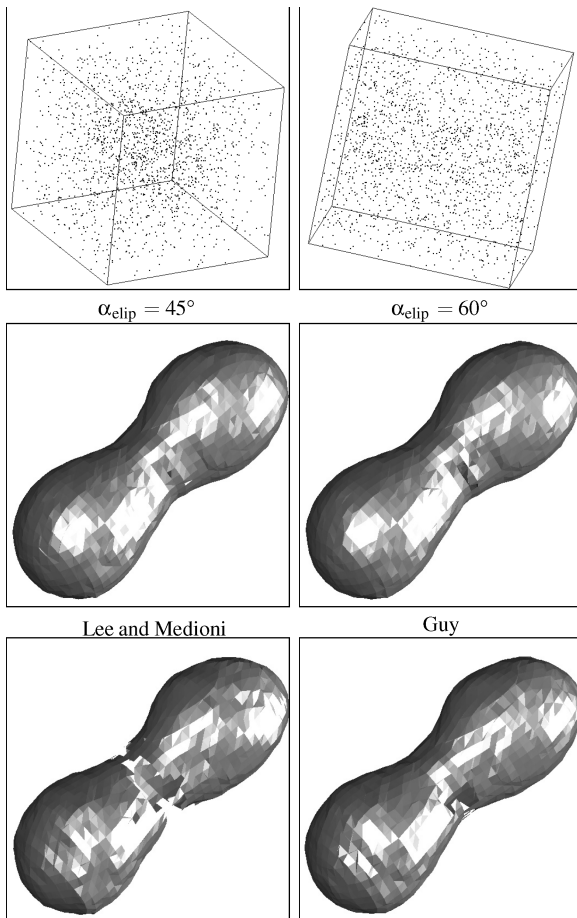


Figure 5: Noisy data example: reconstruction of Cassini's oval in a grid of dimensions $50 \times 50 \times 50$.

balanced pertinence distributions over the surfaces. It is showed in the cut views of the knot model.

The model in Figure 7 is composed by 1330 points. We used $d_{max} = 0.21$ for all methods. The central region of this model is very difficult to reconstruct using the accumulation paradigm presented here. In this region, the ambiguity in normal estimation process results in low pertinence values in contrast with the whole model. All methods incorrectly obtained a hole as a result. In fact, they will fail wherever complex intersections of planes exist.

5.2. Quantitative results

The evaluation of the efficiency or precision of reconstruction methods is a hard task. In some cases it is not even possible because of the difficulty in establishing viable criteria.

In our case, all methods are under the same paradigm and their parameters have the same meanings. It simplifies the

development of a protocol to evaluate the reconstruction of specific surface models.

A reconstructed surface S is composed by k distinct vertices $\{P_1, \dots, P_k\}$ forming triangles. One may estimate the general quality by the *mean squared error* \overline{mse} :

$$\overline{mse}(S, U) = \frac{1}{k} \sum_{i=1}^k \varepsilon^2, \quad \varepsilon = d(P_i, U), \quad (15)$$

where d is the smallest euclidean distance between the vertex P_i and the original surface U .

For precise error evaluation, it is necessary a great number n of samples D_i obtained in the same conditions and representing independent objects M_i of the same class. Expected error average for this class is computed by averaging the individual errors of the reconstructions S_i of D_i :

$$E(\overline{mse}) = \frac{1}{n} \sum_{i=1}^n \overline{mse}(S_i, M_i). \quad (16)$$

Objects M_i may have different orientations and shapes but must represent the same structure. Samples should have the same spatial features such as density and distribution.

Mean squared error estimates (equation (15)) are only valid for good approximations of the original object. Note that the closest point of P_i is not necessarily its homologue in the original surface. Besides, S_j can be a partial reconstruction of M_j and also have low average error.

We observed that the number of triangles of invalid reconstructions diverges from the average of all reconstructions. These rare surfaces must be excluded from the expected error calculation (equation (16)). We use the average \bar{t} and standard-deviation σ_t of number of triangles obtained from n samples

$$\bar{t} = \frac{1}{n} \sum_{i=1}^n t_i, \quad \sigma_t = \sqrt{\frac{1}{n} \sum_{i=1}^n t_i^2 - \bar{t}^2}, \quad (17)$$

to indicate the range $\bar{t} \pm b\sigma_t$ defining valid reconstructions. A surface S_j is rejected if $t_j < \bar{t} - b\sigma_t$ or $t_j > \bar{t} + b\sigma_t$. The adaptive threshold with $b = 2$ proved to be efficient to exclude invalid reconstructions.

5.3. Evaluating ellipsoid reconstruction

Evaluation is made by reconstructing ellipsoids with several shapes and orientations. The goal is to show methods behavior with surfaces having variable curvature. Thus, the slope variation of error curves are much more important than comparing directly the error values (Figure 8).

Every sample is generated by the application of a linear operator on 250 points uniformly distributed over the unit sphere. These linear operators are symmetric positive matrices. Eigenvalues indicate the size of ellipsoid axis. The

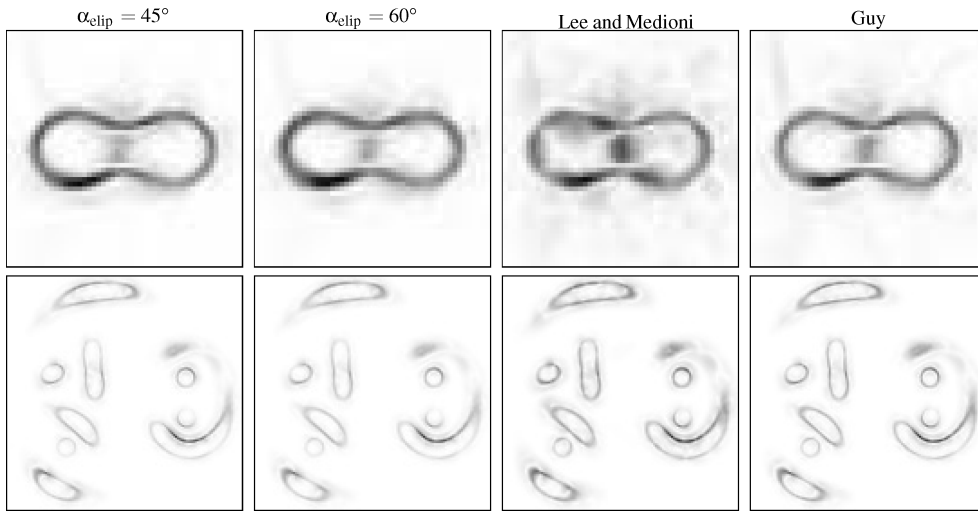


Figure 6: Cut view of the discrete grids illustrating the normalized pertinence of normal inference. Darker points have greater pertinences.

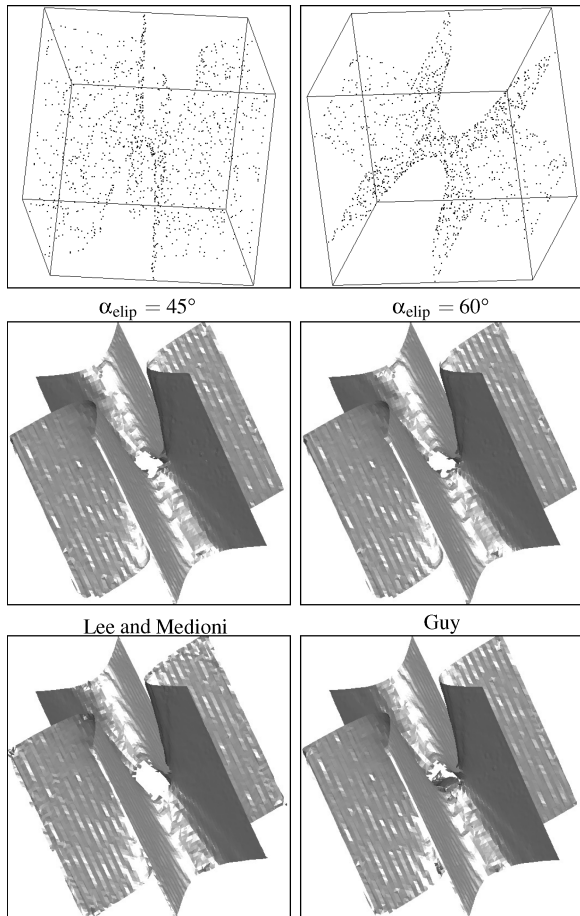


Figure 7: Flaw case example: reconstruction of a complex junction of surfaces in a grid of dimensions $60 \times 60 \times 60$.

greatest eigenvalue is chosen randomly in the range $[1, 1.4]$ and the smallest between $[0.6, 1]$. We fix the intermediary eigenvalue in 1. Eigenvectors define the axis orientation and are also determined randomly.

The change of points density caused by the transformation does not affect the reconstructions. We use a discrete grid of dimensions $40 \times 40 \times 40$.

Figure 8(a) shows the evolution of error in function of $dmax$. High values of $dmax$ can generate bad surfaces because the increase of cross-talking between distant points. For ellipsoid reconstruction, the high curvature regions at extremities get smoother, which explains the error augmentation. Based on these results, we fixed $dmax = 0.33$ for all methods in Figure 8(b,c) since it provides good reconstructions and low cross-talking.

Our method with $\alpha_{clip} = 45^\circ$ provides a better approximation of the high curvature regions obtaining smaller error estimates. For $dmax > 0.03$, the Guy, Lee and $\alpha_{clip} = 60^\circ$ methods have the same behavior. Note that Lee’s method does not provide good results with low values of $dmax$.

Error evolution with number of outliers varying between 250 and 1000 is showed in Figure 8(b). Our method provided better results due to the morphological normal inference. Guy and Lee methods have the same behavior until 150% of outliers. Beyond this limit, the results of Lee’s method are better. With high noise rates, the tangent propagation of Lee’s method enforces the location of surfaces.

Figure 8(c) shows the error evolution in function of additive noise with normal distribution. The evolution of Guy and Lee curves indicates that their methods have similar behavior. The displacement of Lee’s curve does not mean lower sensibility to noise. Our method presents a smaller evolution of error

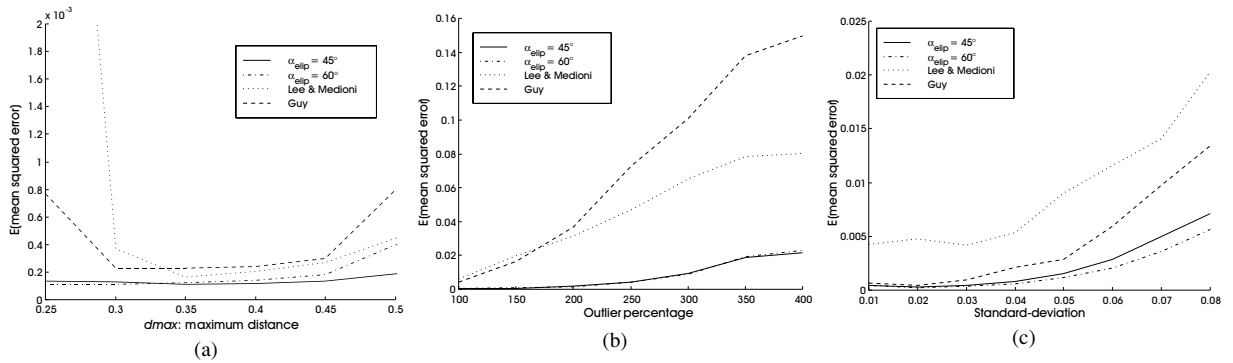


Figure 8: Error curves for ellipsoid reconstruction. (a) Varying the maximum distance d_{max} . Average of 150 samples for each d_{max} . (b) Varying the number of outliers. Average of 122 samples for each noise level. (c) Varying the standard deviation of additive noise. Average of 236 samples for each standard deviation.

average. The method with $\alpha_{\text{ellip}} = 60^\circ$ gives slightly better results than with $\alpha_{\text{ellip}} = 45^\circ$.

6. Conclusions

We have presented a method for robust normal inference based on a specific interpretation of the orientation tensor, an appropriated construction of a tensor field for being a surface structuring element, and a new morphological normal inference process.

Our results show that it is less sensible to noise and to parameters variation, giving more balanced pertinence distributions. The resulting normal estimator functions for the sparse input set can be used for direct surface reconstruction. However, we believe that the combination of this normal estimator with other surface reconstruction methods is promising for future works.

Analyzing the qualitative results, we conclude that our method provides smoother and more stable surfaces. In some cases, it was the unique method able to correctly reconstruct the models (Figure 5). In Figure 4, a correct reconstruction was only possible using elliptic curvature $\alpha_{\text{ellip}} = 60^\circ$.

The Cassini's oval reconstruction and the error evolution varying the number of outliers (Figure 8(b)) demonstrate the positive effects of our morphological operator. It reduces the pertinence of nonstructured points, which explains the good performance of our method with noisy samples. Balanced pertinence estimates are responsible for the lower sensibility of the method to d_{max} variations (Figure 8(a)).

Elliptic trajectories are proposed to adjust the method to different surface curvatures. The reconstruction of samples with additive noise (Figure 8(b)) shows that smaller curvature implies smoother results ($\alpha_{\text{ellip}} > 45^\circ$). In general, circular connections have the best compromise between smoothness and detail preservation ($\alpha_{\text{ellip}} = 45^\circ$). A more powerful ap-

proach is to adaptively match the normal tensor field curvature with each local patch curvature.

Our results were obtained without using a discrete normal tensor field in the reconstruction step. The probabilistic approach described in Section 4.1 to reduce structural aliasing is a subject for future works.

A method for curve reconstruction can be defined by the same ideas of this work. Also, better results may be obtained by developing new structuring tensor fields, iterative operators and heuristics for organization inference.

Acknowledgment

The authors are grateful to CAPES-Brazil/COFECUB and CNPq-Brazil for the financial support to this work.

References

1. H. Hoppe. *Surface Reconstruction from Unorganized Points*. Ph.D. thesis, University of Washington, 1994.
2. N. Amenta, M. Bern and M. Kamvysselis. A new voronoi-based surface reconstruction algorithm. In *SIGGRAPH*, pp. 415–421, 1998.
3. M. Gopi and S. Krishnan. A fast and efficient projection-based approach for surface reconstruction. *High Performance Computer Graphics, Multimedia and Visualization 1*(1):1–12, 2000.
4. G. Guy. *Inference of Multiple Curves and Surfaces from Sparse Data*. Ph.D. thesis, IRIS/University of Southern California, 1996.
5. G. Medioni, M.-S. Lee and C.-K. Tang. *A Computational Framework for Segmentation and Grouping*, first edition. Elsevier Science B.V., 2000.

6. M.-S. Lee and G. Medioni. Grouping \cdot , \cdot , \rightarrow , 0 , into regions, curves, and junctions. *IEEE Computer Vision and Image Understanding* 76(1):54–69, October 1999.
7. H. Knutsson. Representing local structure using tensors. In *The 6th Scandinavian Conference on Image Analysis*, Oulu, Finland, pp. 19–22, June 1989.
8. J. Carr, R. Beatson, B. McCallum, W. Fright, T. McLennan and T. Mitchell. Smooth surface reconstruction from noisy range data. In *ACM GRAPHITE*, pp. 119–297, 2003.
9. J. Carr, R. Beatson, J. Cherrie, T. Mitchell, W. Fright, B. McCallum and T. Evans. Reconstruction and representation of 3D objects with radial basis functions. In *SIGGRAPH*, pp. 67–76, 2001.
10. M. B. Vieira. *Orientation Inference of Sparse Data for Surface Reconstruction*. Ph.D. thesis, Universidade Federal de Minas Gerais (Brazil) and Université de Cergy-Pontoise (France), 2002.
11. C.-F. Westin. A Tensor Framework for Multidimensional Signal Processing. Ph.D. thesis, Linköping University, Sweden, 1994.
12. M. B. Vieira, M. Cord, P. P. Martins Jr., S. Philipp-Foliguet and A. Araújo. Filtering sparse data with 3D tensorial structuring elements. In *proceedings of SIB-GRAPI* Fortaleza, Brazil, October 2002.
13. M. Cord, M. Jordan, T. Belli and M. B. Vieira. Analyse d’images aériennes haute résolution pour la reconstruction de scènes urbaines. *Société Française de Photogrammétrie et Télédétection*, 166:34–43, 2002.
14. N. Amenta and Y. J. Kil. Defining point-set surfaces. In *SIGGRAPH*, pp. 264–270, 2004.